# Supporting Information

# $\pi$-Conjugation and Endgroup Effects in Long Cumulenes: Raman Spectroscopy and DFT Calculations

Matteo Tommasini,*,† Alberto Milani,† Daniele Fazzi,‡ Andrea Lucotti,† Chiara Castiglioni,† Johanna A. Januszewski,¶ Dominik Wendinger,¶ and Rik R. Tykwinski¶

*Dipartimento di Chimica, Materiali e Ingegneria Chimica – Politecnico di Milano, Piazza Leonardo da Vinci, 32 – 20133 Milano (Italy), Max-Planck-Institut für Kohlenforschung, Kaiser-Wilhelm-Platz 1,45470 Mülheim (Germany), and Department of Chemistry and Pharmacy & Interdisciplinary Center of Molecular Materials (ICMM), Friedrich-Alexander-Universität Erlangen-Nürnberg (FAU), Henkestrasse 42, 91054 Erlangen (Germany)*

E-mail: matteo.tommasini@polimi.it

*To whom correspondence should be addressed

†Dipartimento di Chimica, Materiali e Ingegneria Chimica – Politecnico di Milano, Piazza Leonardo da Vinci, 32 – 20133 Milano (Italy)

‡Max-Planck-Institut für Kohlenforschung, Kaiser-Wilhelm-Platz 1,45470 Mülheim (Germany)

¶Department of Chemistry and Pharmacy & Interdisciplinary Center of Molecular Materials (ICMM), Friedrich-Alexander-Universität Erlangen-Nürnberg (FAU), Henkestrasse 42, 91054 Erlangen (Germany)

October 10, 2014

# Contents



# DFT calculations of the vibrational spectra

We discuss here in details the results of DFT calculations of the vibrational spectra of [$n$]tBuPh and [9]Mes. The comparison between computed and experimental IR spectra is reported in Figure SI.1 for three molecules of the series showing that the overall pattern of the main IR features is reproduced quite well by the calculations. However, some discrepancies between theory and experiments should be described.

(i) Even if the commonly accepted frequency-scaling factor of 0.9594[1] has been applied, the bands above 1800 $cm^{-1}$ (assigned to CC stretching modes of the cumulene chain) are still predicted at higher wavenumber than the corresponding experimental signals. (ii) For [7]tBuPh a doublet is predicted around 1600 $cm^{-1}$: The higher frequency peak does not find an evident correspondence in the experimental spectrum; however it should be correlated to one of the components of the strong and structured experimental band located at 1589 $cm^{-1}$.

Since DFT vibrational force fields show some weakness in describing extended $\pi$- conjugated linear chains, a good match with experimental CC stretching frequencies can be reached only after applying scaling factors which are properly chosen on the basis of the length of the conjugated chain, as reported in.[2] Inaccuracies in the description of the CC stretching force constants (notably interaction terms) are likely responsible of the appearance of the higher wavenumber component of the doublet at about 1600 $cm^{-1}$ in the predicted spectrum. In fact, the associated normal mode (see Figure SI.2) involves both ring stretching and CC stretching of the sp-chain, the latter leading to an overesti-

mation of the vibrational wavenumber. The associated experimental band is most likely found at lower wavenumber and may be coincident with the strong and structured feature observed at 1586 $cm^{-1}$.

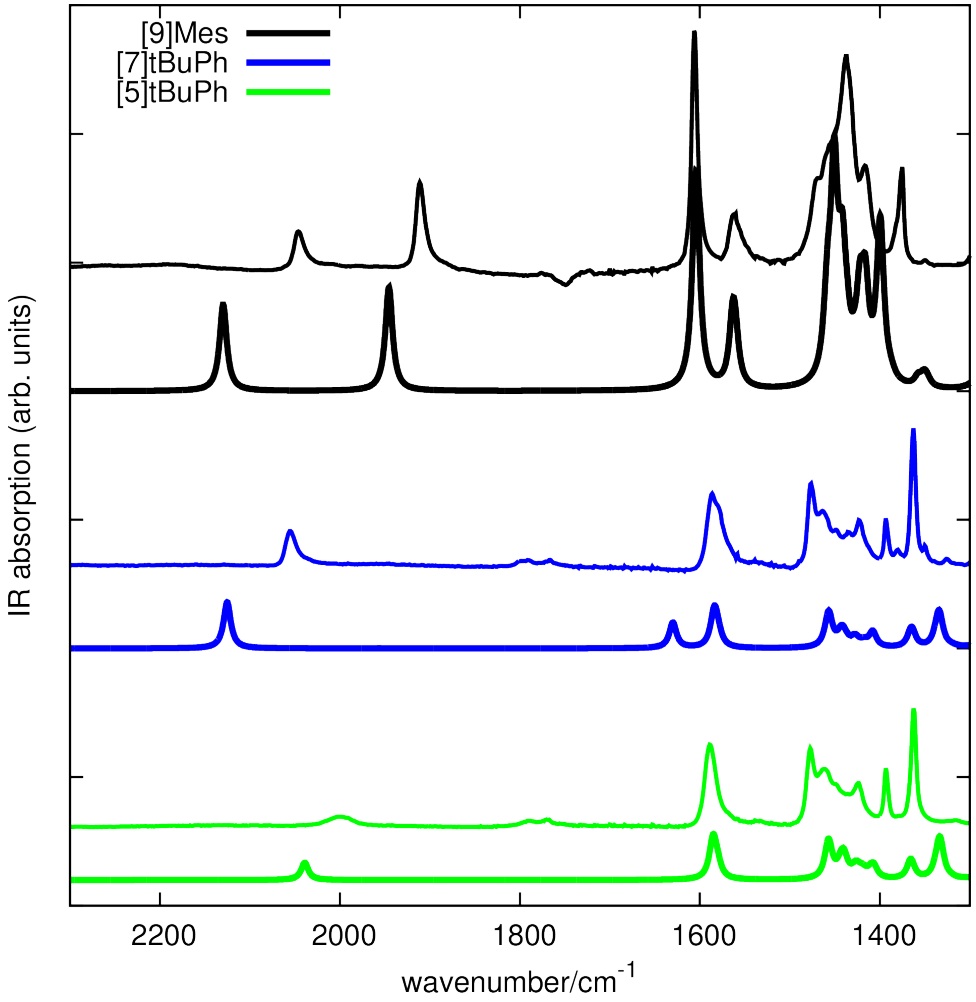


Figure SI.1: Comparison between experimental (thin lines) and theoretical (thick lines) infrared spectra of [5]tBuPh, [7]tBuPh and [9]Mes. Frequency scaling factor adopted for theoretical spectra: 0.9594.[1] The same intensity scale has been used for the plot of calculated spectra, while the intensity scale of each experimental spectrum has been adjusted to the corresponding calculated spectrum. Experimental spectra from solid samples.

From Figure SI.1 we also observe that [9]Mes shows a remarkable overall enhancement of the computed infrared intensities with respect to [5]tBuPh and [7]tBuPh ([5]tBuPh and [7]tBuPh instead display similar computed intensity values for the main IR transitions). This effect is related to polarization of CC bonds in the aryl rings, resulting in charge delocalization via hyperconjugation with the methyl groups, which is a peculiar feature of the Mes caps compared to tBuPh caps.

The experimental and computed Raman spectra of [$n$]tBuPh series and [9]Mes are shown in Figure SI.2. The theoretical predictions always overestimate the Raman activity and the frequency of the $\mathcal{R}$ mode. The discrepancy, both in frequency and intensity, progressively increases with chain length. A viable way to recover the correct intensity pattern is to adopt a suitable scaling of the polarizability ($\boldsymbol{\alpha}$) derivatives with respect to the CC stretching coordinates of the cumulene chain (*i.e.* Tr($d\boldsymbol{\alpha}/dR_{C=C}$) parameters); see the following section for a discussion.

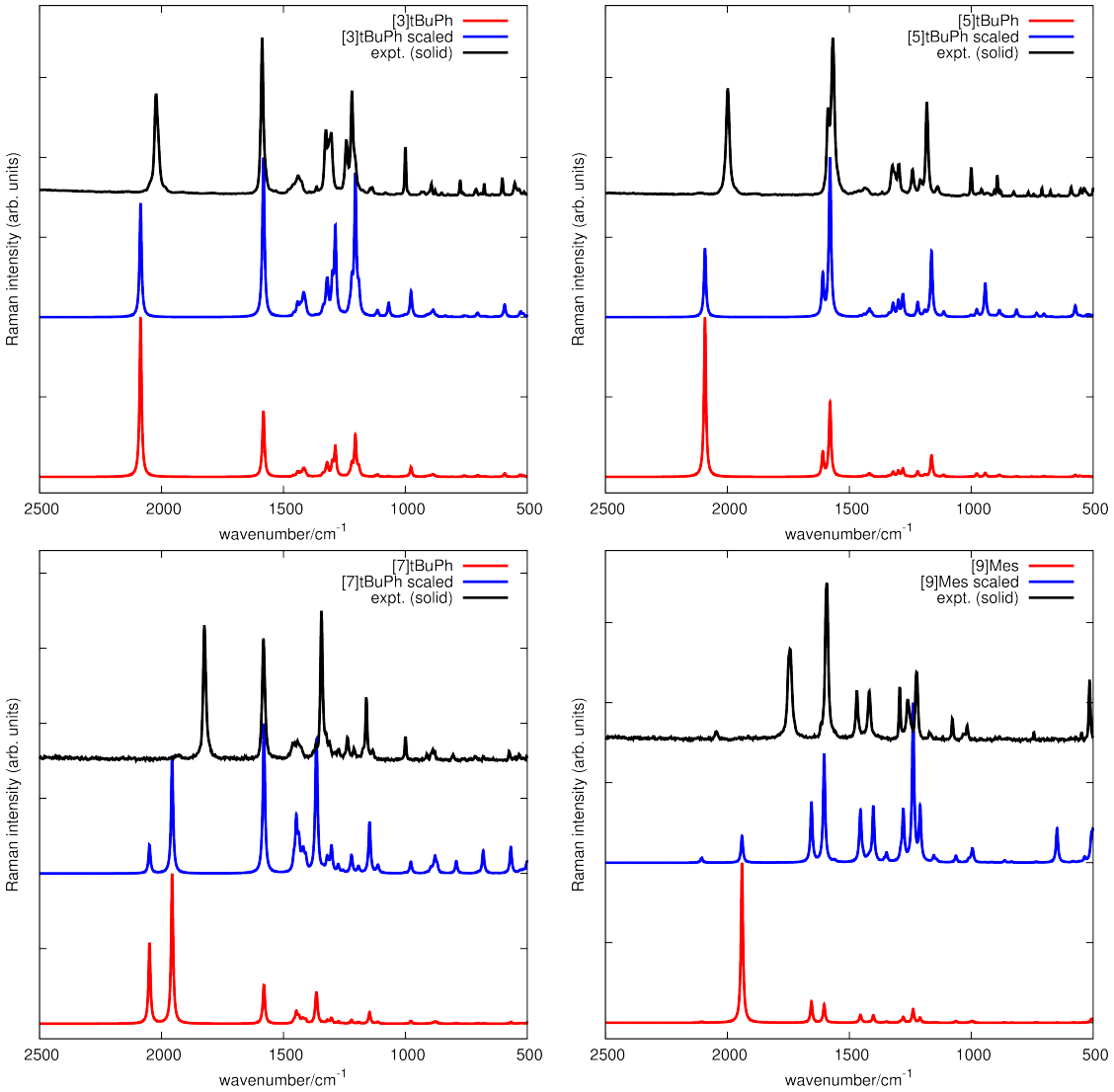


Figure SI.2: Comparison between experimental and theoretical (PBE0/6-311G**) Raman spectra of [$n$]tBuPh and [9]Mes. Frequency scaling factor applied to theoretical spectra: 0.9594.[1] Experimental spectra from solid samples. Theoretical spectra plotted with a blue line (spectra in the middle) have been obtained after scaling of the intensity parameters relative to the cumulene chain.

In this way it is possible to recover the correct spectral pattern (in terms of intensity dis-

tribution among the different Raman active transitions). The adopted procedure requires that the polarizability ($\alpha$) derivatives with respect to the CC stretching coordinates of the cumulene chain (*i.e.* $d\boldsymbol{\alpha}/dR_{C=C}$ parameters) are scaled with a different factor $x_n$, with decreasing values while $n$ increases (the values $x_3 = 0.45, x_5 = 0.3, x_7 = 0.2, x_9 = 0.09$ have been used for [3,5,7]tBuPh and 9[Mes]). The need of different scaling factors for chains with different length confirms that the increasing trend of $\mathcal{R}$ mode intensities for increasing sp-chain length is too steep.

On the other hand, the predicted intensity pattern of the ring stretching bands nicely follows the experimental trend (see Table SI.1). In Table SI.1 we report quantitative data obtained by the analysis of the integrated Raman intensities (normalized to CH stretching intensities) of SP[$N$] and [$n$]tBuPh. The $\mathcal{R}$ line and two selected Raman lines of the aryl groups, namely the ring stretching line at about 1600 cm$^{-1}$ and the ring breathing at about 1000 cm$^{-1}$. These data allow a direct comparison between cumulenes and polyynes and support the hypothesis of a strong electrical coupling between aryl rings and carbon chain in cumulenes.

Let us focus on the Raman spectra of [7]tBuPh and SP[4] (Figure 6 and Table SI.2) to better assess the outcome of the theoretical predictions. DFT indicates that the transition associated to $\mathcal{R}$ vibrations of [7]tBuPh exhibits a Raman activity whose strength is comparable (same order of magnitude) to that of SP[4] (see Table SI.2). However, comparing with the corresponding experimental data (Table SI.2), the predicted Raman intensity of the $\mathcal{R}$ modes is too high both for the cumulene and the polyyne: the $I_{\mathcal{R}}/I_{CH}$ ratios are overestimated by a factor of about 3 in both cases. Figure 6 shows that the computed $\mathcal{R}$ mode frequencies of the two molecules follows the experimental trend, characterized by a remarkable lowering of its wave-number in the case of cumulenes. However the observed frequency shift ($\Delta\nu$ = 400 cm$^{-1}$) is underestimated by calculations ($\Delta\nu$ = 235 cm$^{-1}$). Moreover, DFT calculations on [7]tBuPh predict two distinct strong Raman lines located around 2000 cm$^{-1}$, while in the experimental spectrum just one strong Raman line occurs, accompanied by a weak feature at higher wavenumber[1]. While the

[1]The two features predicted near 2000 cm$^{-1}$ are due to normal modes with large $\mathcal{R}$ content, but the

**Table SI.1: Relative Raman intensities in SP[$N$] polyynes and [$n$]tBuPh cumulenes for $\mathcal{R}$, ring-stretching and ring-breathing lines from experiments and DFT predictions. Normalization of experimental intensities was carried out with respect to the signal in the aliphatic CH stretching region (2820 – 3025 cm$^{-1}$), which is assumed to be stable with respect to $\pi$-conjugation effects and is due to similar end-groups in the two series. In [9]Mes the aliphatic CH bonds are a total of 36, while in [$n$]tBuPh series they are 72. In SP[$N$] polyynes the number of aliphatic CH is 108.**

| (a) | N | #CC | $\nu_{\mathcal{R}}$ cm$^{-1}$ | $I_{\mathcal{R}}/I_{CH}$ expt. | $I_{\mathcal{R}}/I_{CH}$ DFT | ring str./CH expt. | ring str./CH DFT | ring breath./CH expt. |
|---|---|---|---|---|---|---|---|---|
| SP[4] | 4 | 7 | 2152 | 6.3 (9.45[c]) | 17.24 (25.86[c]) | 0.1 | 0.06 | 0.2 |
| SP[6] | 6 | 11 | 2084 | 42.7 (64.05[c]) | - | 0.2 | - | 0.3 |
| SP[8] | 8 | 15 | 2017 | 58.0 (87.00[c]) | - | 0.2 | - | 0.2 |
| SP[10] | 10 | 19 | 1981 | 177.0 | - | 0.2 | - | 0.5 |
| SP[12] | 12 | 23 | 1958 | 209.3 | - | 0.2 | - | 0.2 |
| (b) | n | #CC | $\nu_{\mathcal{R}}$ cm$^{-1}$ | $I_{\mathcal{R}}/I_{CH}$ expt. | $I_{\mathcal{R}}/I_{CH}$ DFT | ring str./CH expt. | ring str./CH DFT | ring breath./CH expt. |
| [3]tBuPh | 3 | 3 | 2023 | 2.5 | 3.9 | 2.5 | 1.7 | 0.4 |
| [5]tBuPh | 5 | 5 | 1997 | 6.1 | 16.2 | 11.3 | 10.3 | 0.6 |
| [7]tBuPh | 7 | 7 | 1824 | 15.1 | 51.2 | 13.5 | 9.3 | 1.6 |
| [9]Mes | 9 | 9 | 1743 | 31.9 (15.9[d]) | 67.5 | 41.8 (20.9[d]) | 16.5 (8.2[d]) | 3.9 (1.9[d]) |

(a) In SP[$N$] the ring stretching frequency is located at 1597 cm$^{-1}$ and the ring breathing is located at 1003 cm$^{-1}$.

(b) Ring stretching in cumulenes (cm$^{-1}$): 1587 (n = 3); doublet 1587, 1567 (n = 5); 1582 (n = 7); 1593 (n = 9). Ring breathing in cumulenes (cm$^{-1}$): 1000 (n = 3, 5, 7); doublet 1016, 1032 (n = 9). To increase the signal-to-noise ratio in the aliphatic CH stretching region of [$n$]tBuPh (n = 7, 9) we have considered the average of the spectra taken at earliest times within the first 30 minutes right after solvent evaporation (further details in the Experimental section of the main text).

(c) Intensity data for SP[$N$] are referred to the CH stretching intensity of 108 aliphatic CH oscillators, while in [$n$]tBuPh the number of aliphatic CH oscillators is 72. Hence to compare SP[$N$] data on the same ground as [$n$]tBuPh one has to multiply $I_{\mathcal{R}}/I_{CH}$ of SP[$N$] by 1.5 = 108/72.

(d) Intensity data for [9]Mes are referred to the CH stretching intensity of 12 methyl groups, while in the [$n$]tBuPh series the methyl groups are 24. To ease the comparison with [$n$]tBuPh data, re-normalized intensity ratios (factor of 2) for [9]Mes are reported in parentheses.

**Table SI.2: Comparison of $I_{\mathcal{R}}/I_{CH}$ intensity ratios in [7]tBuPh and SP[4]: summary of the Raman intensity data from DFT and experimental data (see also Table SI.1).**

| | [7]tBuPh | SP[4] |
|---|---|---|
| DFT | 51.2 | 17.24 |
| Expt. | 15.1 | 6.3 |

theoretically predicted behavior of the $\mathcal{R}$ mode of sp chains is lacking under some regards, the good accordance between the theoretically predicted spectrum and experiments in the ring stretching region allows to rationalize the unusual Raman intensity enhancement observed in this region in the case of cumulene species. The eigenvectors relative to the main Raman lines computed in the 1520 – 1420 $cm^{-1}$ region are reported in Figure SI.3. In particular, we can focus on the modes at 1647 $cm^{-1}$, at 1508 $cm^{-1}$, at 1420 $cm^{-1}$ and 1195 $cm^{-1}$. As expected (see above), these modes involve both CC stretching localized on the aryl rings and CC stretching of the chain. While the higher frequency mode carries a contribution from the chain restricted to the most peripheral CC bonds, the normal modes occurring at 1508 $cm^{-1}$ (1447 $cm^{-1}$ after scaling) at 1420 $cm^{-1}$ (1362 $cm^{-1}$ after scaling) and 1195 $cm^{-1}$ (1146 $cm^{-1}$ after scaling), should be classified as a chain modes, due to the collective character of the vibrational displacement of the chain, involving the whole sequence of sp carbon atoms. In this regard it is worthwhile to mention that the experimental lines observed below 1500 $cm^{-1}$ (associated to the modes just described) do not have a counterpart in the Raman spectrum of polyynes since longitudinal modes of polyyne chains are found at higher frequencies.

## Discussion on computed Raman intensities

The fact that DFT calculations partially fail to represent correctly the relative Raman intensity of $\pi$-conjugation dependent modes in sp-carbon chains indicates that present DFT functionals (at least those most popular in theoretical spectroscopy) cannot fully cope with highly $\pi$-conjugated systems, since their properties are very finely tuned by the molecular structure (*i.e.* by chain length, BLA pattern) and, more importantly, by the electronic coupling with the end groups. However, it is fairly challenging to model the subtle interplay among all the mentioned parameters employing explicitly correlated

two are differently localized along the sp-chain: one (computed at 2039 $cm^{-1}$ – scaled value: 1956 $cm^{-1}$) shows larger displacements over the peripheral CC bonds while the other (2135 $cm^{-1}$ – scaled value: 2048 $cm^{-1}$) is more localized in the center of the sp-chain. However, while DFT grants high intensity to both modes, experimentally the mode at higher frequency is markedly weaker than that at lower frequency.

2136 $cm^{-1}$; 0 km/mol; 116096 $A^4$/amu

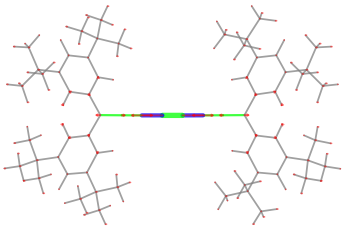

2039 $cm^{-1}$; 0 km/mol; 206102 $A^4$/amu

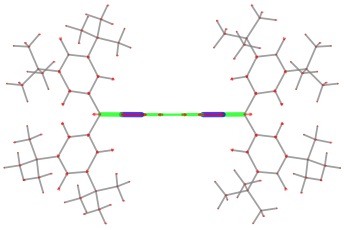

1699 $cm^{-1}$; 117 km/mol; 8 $A^4$/amu

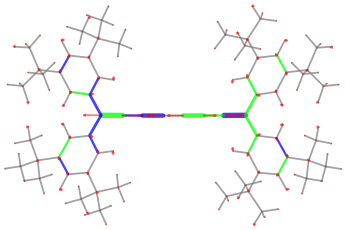

1647 $cm^{-1}$; 5 km/mol; 27153 $A^4$/amu

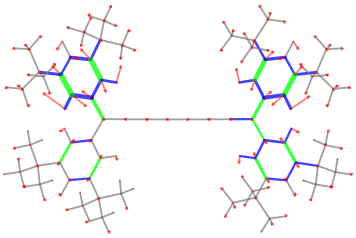

1508 $cm^{-1}$; 4 km/mol; 10892 $A^4$/amu

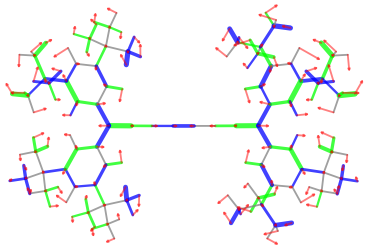

1420 $cm^{-1}$; 0 km/mol; 12848 $A^4$/amu

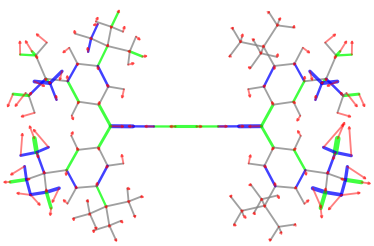

1195 $cm^{-1}$; 0 km/mol; 9275 $A^4$/amu

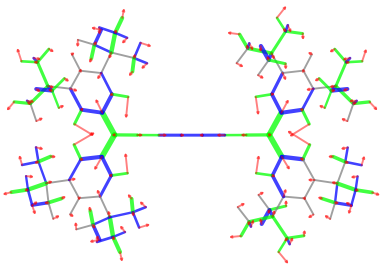

Figure SI.3: Representation of nuclear displacements for selected normal modes of [7]tBuPh (PBE0/6-311G** calculations). Red arrows represent displacement vectors; CC bonds are represented as green (blue) lines of different thickness according to their relative stretching (shrinking).

quantum chemistry for the prediction of the Raman response. This is due to the size of the systems investigated, which cannot be reduced by assuming simplified chemical structures. The full molecular structure is required in the quantum chemical models in order to correctly include the fine details of the end groups. On the other hand, this fact clearly highlights the peculiar chemical physical behavior of these molecular species, characterized by a highly delocalized, quasi metallic $\pi$ system: they are prone to a sudden modulation of their properties (*e.g.* in terms of molecular geometry, electronic structure and spectroscopic response) by relatively little changes of their chemical structure, as for instance by the choice of different end groups or a further functionalization of them or even by conformational changes. This latter point deserves a brief comment, since conformational differences of the aryl caps are observed in [9]Mes compared to [7]tBuPh. In [9]Mes the aryl twist angles of the mesityl groups (see Figure 1 of the text for their definition) are about 50° in solid state,[3] which limits conjugation between the aryl ring and the chain of sp-hybridized carbon atoms with respect to [7]tBuPh, where at each terminus, the twist angle for one aryl ring is significantly smaller (average 19°) than that of the other (average 49°).[3] Interestingly, while DFT correctly evaluate the twist angle in [9]Mes (49°), it does not distinguish the different conformation of the two twist angles in [7]tBuPh (just one twist angle is found at 31°), presumably because molecular packing effects are absent in the isolated model molecule. Nevertheless the change of twist angle from [9]Mes to [7]tBuPh affects the amount of aryl-sp-chain interaction: the frontier orbital maps (Figure 7) display slightly less sp-chain/aryl mixing for [9]Mes than [7]tBuPh, as expected.[3] Consistently, due to different sp-chain/aryl interaction, the otherwise degenerate HOMO-1/HOMO levels (*e.g.* in vinylidene endcapped cumulenes[4]) are closer in [9]Mes than in [7]tBuPh.

# Pattern of CC bond polarizability derivatives in sp-chains

A look at the $\mathrm{Tr}(d\boldsymbol{\alpha}/dR_j)$ parameters reported in Figure 9 of the main text shows a non-negligible difference between SP[4] and [7]tBuPh. While in SP[4] we find positive $\mathrm{Tr}(d\boldsymbol{\alpha}/dR_j)$ values for the shorter bonds, *i.e.* when $R_j$ corresponds to a triple bond of the structure formula (for instance bond #1, see Figure 2.b) and negative values for the longer ones (*i.e.* "single" CC bonds, as bond #2), the parameters $\mathrm{Tr}(d\boldsymbol{\alpha}/dR_j)$ of [7]tBuPh show the opposite trend with respect to the bond lengths pattern. Indeed, signs of $\mathrm{Tr}(d\boldsymbol{\alpha}/dR_j)$ are concordant for SP[4] and [7]tBuPh even though the BLA pattern is opposite (see Figure 2b). In this light the behavior of [7]tBuPh results to be twofold anomalous, namely: (i) it shows large values and a saw tooth pattern of $\mathrm{Tr}(d\boldsymbol{\alpha}/dR_j)$, while the chain presents a "quasi" equalized structure; (ii) it does not follows the usual correlation (in sign) with individual CC bond lengths. We can rationalize the origin of such behavior looking at molecular orbitals (see Figure 7) and analyzing in details their role in determining both molecular structure and Raman activity. In $\pi$-conjugated systems the pattern of nodes of the HOMO orbitals usually determines how "single" (longer) and "double/triple" (shorter) bonds are localized. This pattern is indeed followed by the actual ground state molecular structure, as it can be verified for oligoenes, polyynes, and also more complex systems as polycyclic aromatic hydrocarbons.[5] For instance, the two degenerate HOMO orbitals of SP[4], which can be described as $\pi_x$ and $\pi_y$ orbitals, shows the identical nodal behavior, with nodes in the middle of CC bonds at even sites, *i.e.* located on the "single" CC bonds of the structure formula. The case of [7]tBuPh is markedly different. First of all, the degeneracy of the frontier orbitals is effectively removed because of the different coupling with $2p$ electrons of the aryl moieties: $\pi$-conjugation extends more and differently in HOMO with respect to HOMO-1, due to the coupling between $2p_x$ orbitals of the chain and $2p$ orbitals of the aryl rings. The nodal pattern of HOMO parallels that of the HOMO of SP[4], with nodes on the odd bonds. On the opposite, the $2p_y$ orbitals of the sp chain concur to the formation of a $\pi_y$ HOMO-1 molecular orbital, which is

practically confined just on the sp chain. In [7]tBuPh, at difference from HOMO, the HOMO-1 does provide bonding contributions to the odd bonds since nodes are in this case at the even sites. Hence, bonding contributions from HOMO are counter acted by anti-bonding contributions arising from HOMO-1 and vice versa, effectively driving [7]tBuPh toward an almost vanishing bond length alternation pattern. As a consequence, contrary to oligoenes and polyynes, the nodal pattern of the HOMO of aryl cumulenes is such that it does not comply with the (small) bond length alternation pattern: indeed the nodal planes of HOMO do correspond to those bonds which in fact are slightly shorter. As it will be proven in the following discussion, this is the very reason why, at difference from polyynes, the bond length pattern shown by [$n$]tBuPh does not correlate with the sign of the Tr($d\boldsymbol{\alpha}/dR_j$) parameters. The relationship between Raman parameters and electronic structure can be analyzed within a simple Hückel approach to $\pi$-conjugated systems. This approach has the benefit of being simple and provides a straightforward clue to the interpretation of the present data. In[6] it was shown that:

$$\frac{\partial \alpha_{uv}}{\partial R_j} \propto \left(\frac{\partial \beta}{\partial R}\right) \sum_e \left[\delta P_j^{ge} \, \frac{\mu_u^{ge} \mu_v^{ge}}{\Delta E_{ge}^2}\right] \tag{1}$$

where $\delta P_j^{ge}$ represents the bond order change of the j-th $\pi$-conjugated bond upon transition from ground (g) to an excited state (e). This quantity evaluated within Hückel theory gives:

$$\delta P_j^{ge} = C_{\lambda k'} C_{\nu k'} - C_{\lambda k} C_{\nu k} \tag{2}$$

where $C$ are the MO coefficients, $\lambda$, $\nu$ are the nearest neighbor atomic orbitals at bond $j$, and $k$, $k$ are the occupied and virtual orbitals defining the excitation $e$. It is evident that the signs of the Raman parameters are directly determined by the bond order change upon excitation $\delta P$, hence by the coefficients of the MOs involved in the lowest dipole allowed electronic transition which provides the leading term in the sum over $e$. This is usually described as mainly due to the HOMO-LUMO excitation. Inspection of the HOMO/LUMO orbital maps (see also the nodal analysis reported in Figure SI.4) provides the rationalization of the alternated behavior of the Raman parameters. For instance,

let us consider the CC bond #1 located between carbon atoms 1 and 2: it is described as a triple bond in the conventional polyyne structure formula. In SP[4] the product $C_{1LUMO}C_{2LUMO}$ is negative, as for [7]tBuPh, while the term $C_{1HOMO}C_{2HOMO}$ is positive. By consequence, based on Eq. (2), $\delta P^{ge}$ of CC bond #1 is negative for the two molecules. In fact, upon HOMO $\rightarrow$ LUMO transition, CC bond #1 receives an anti-bonding contribution both in SP[4] and [7]tBuPh. Since $d\beta/dR < 0$, based on Eq. (1) we conclude that the Raman bond parameter of bond #1 is positive. The opposite happens for CC bond #2 which carries negative values of $\mathrm{Tr}(d\boldsymbol{\alpha}/dR_j)$, since upon electronic excitation it receives a bonding contribution as one can easily realize by looking at the orbital maps of Figure SI.4. Notice that the case of [9]Mes perfectly parallels the behavior found for [7]tBuPh (see Figure SI.4 and Figure 8 of the main text).

The above discussion allows to understand why, independently on the different bond length pattern, SP[4] and [7]tBuPh show similar Raman parameters and consequently strong and comparable Raman intensity of the $\mathcal{R}$ mode: the relevant issue is indeed the leading role of the frontier orbitals in determining the Raman response. The same concepts can be used to justify the very different pattern shown by the local Raman parameters of a vinylidene endcapped cumulene (Figure 9). Also in this case, because of the presence of the $sp^2$ carbons at the ends of the conjugated sequence, the molecule has two distinct HOMO and HOMO-1 (LUMO and LUMO-1) orbitals (see Figure SI.5). However, at difference from aryl capped cumulenes [7]- and [9]tBuPh, showing a sizeable energy gap between HOMO and HOMO-1 (see above), the two pairs of HOMO-1/HOMO orbitals of $CH_2C_6CH_2$ are remarkably closer in energy (respectively: -0.239, -0.236; values in hartree), thus resulting in accidentally degenerate energy levels. The nodal pattern of HOMO and HOMO-1 orbitals of $CH_2C_6CH_2$ is identical to that of the corresponding orbitals of [7]tBuPh (see for instance Figure SI.5 and compare it with Figure 8 of the main text), and the two orbitals concur in a similar way as for [7]tBuPh to the definition of the equilibrium structure (which is indeed quasi-equalized for both cumulenes). At difference from [7]tBuPh, in $CH_2C_6CH_2$ due to their close energy the two pairs of accidentally degenerate frontier orbitals are simultaneously involved in the lower en-

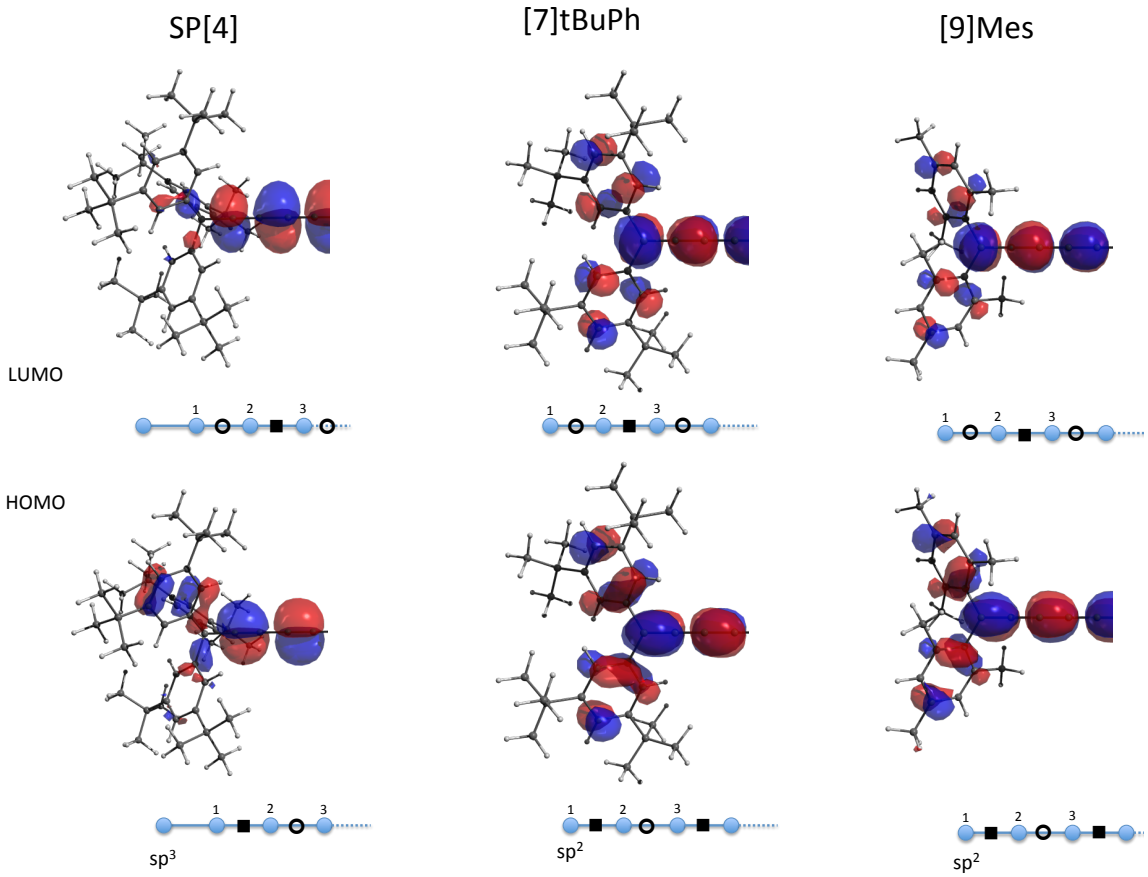


Figure SI.4: Frontier orbitals of SP[4] polyyne (left column), [7]tBuPh (central column) and [9]Mes cumulene (right column). After PBE0/6-311G** DFT calculations (only one half of the molecule is shown). Nodal analysis is provided for each map, starting from the end atom of the conjugated carbon sequence (the one bearing the aryl caps). For a given bond and MO full square indicate a bonding contribution, while open circle indicate an anti-bonding contribution (*i.e.* the presence of a nodal plane orthogonal to the CC bond).

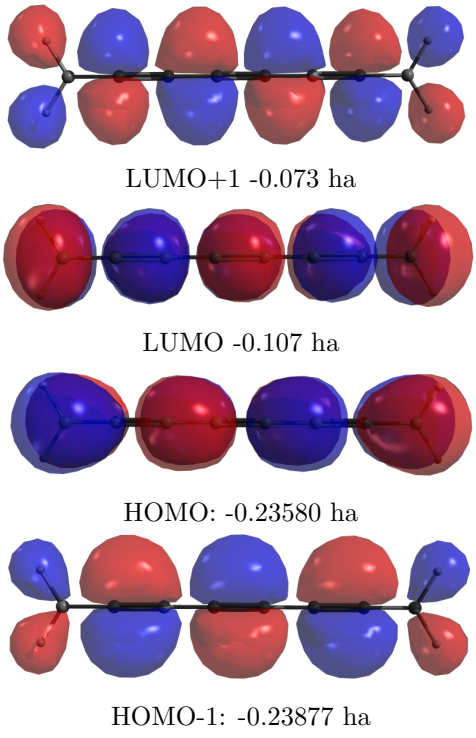


Figure SI.5: Map of HOMO-1, HOMO, LUMO, LUMO+1 orbitals of $CH_2C_6CH_2$ (after PBE0/6-311G** DFT calculations)

ergy electronic transition, which TDDFT describes in terms of both HOMO/LUMO and HOMO-1/LUMO+1 excitations. From the side of the prediction of the Raman response, the relevant point is that both excitations must be included in Eq. (1), giving rise to two distinct contributions (with opposite sign) to any $\mathrm{Tr}(d\boldsymbol{\alpha}/dR_j)$ parameter. This fact justifies the occurrence of local parameters characterized by low values and the loss of the characteristic saw tooth pattern in the $\mathrm{Tr}(d\boldsymbol{\alpha}/dR_j)$ plot. In addition to the cancellation effect by the two opposite contributions, a remarkable lowering of the oscillator strength of the first dipole allowed transition while passing from [7]tBu to $CH_2C_6CH_2$ is theoretically predicted, thus providing a further rationale for the occurrence of low $\mathrm{Tr}(d\boldsymbol{\alpha}/dR_j)$ values in vinylidene endcapped cumulenes.

## References

(1) Merrick, J. P.; Moran, D.; Radom, L. An Evaluation of Harmonic Vibrational Frequency Scale Factors. *J. Phys. Chem. A* **2007**, *111*, 11683–11700.

(2) Tommasini, M.; Fazzi, D.; Milani, A.; Del Zoppo, M.; Castiglioni, C.; Zerbi, G. Intramolecular Vibrational Force Fields for Linear Carbon Chains through an Adaptative Linear Scaling Scheme. *J. Phys. Chem. A* **2007**, *111*, 11645–11651.

(3) Januszewski, J. A.; Wendinger, D.; Methfessel, C. D.; Hampel, F.; Tykwinski, R. R. Synthesis and Structure of Tetraarylcumulenes: Characterization of Bond-Length Alternation versus Molecule Length. *Angew. Chem., Int. Ed.* **2013**, *52*, 1817–1821.

(4) Innocenti, F.; Milani, A.; Castiglioni, C. Can Raman spectroscopy detect cumulenic structures of linear carbon chains? *J. Raman Spectrosc.* **2010**, *41*, 226–236.

(5) Castiglioni, C.; Tommasini, M.; Zerbi, G. Raman spectroscopy of polyconjugated molecules and materials: confinement effect in one and two dimensions. *Phil. Trans. R. Soc. A* **2004**, *362*, 2425–2459.

(6) Tommasini, M.; Castiglioni, C.; Zerbi, G. Raman scattering of molecular graphenes. *Phys. Chem. Chem. Phys.* **2009**, *11*, 10185–10194.